



ELSEVIER

Physica D 162 (2002) 244–255

**PHYSICA** D

www.elsevier.com/locate/physd

# Nonlinear determinism in time series measurements of two-dimensional turbulence

Mario Ragwitz<sup>a,\*</sup>, Charles N. Baroud<sup>b</sup>, Brendan B. Plapp<sup>b</sup>, Harry L. Swinney<sup>b</sup><sup>a</sup> *Max-Planck Institut für Physik Komplexer Systeme, Nöthnitzer Strasse 38, D 01187 Dresden, Germany*<sup>b</sup> *Department of Physics, Center for Nonlinear Dynamics, University of Texas at Austin, Austin, TX 78712, USA*

Received 4 May 2001; received in revised form 3 September 2001; accepted 5 November 2001

Communicated by E. Kostelich

## Abstract

Experiments on two-dimensional and three-dimensional turbulent flows in a rotating annulus are analyzed using linear and nonlinear time series predictors. The models are used to predict the time series, a time  $S$  ahead and to calculate the velocity increment  $\Delta u_S = u(s_n + S) - u(s_n)$  between the current value of the time series  $s_n$  and a point time  $S$  apart. For two-dimensional flow, the nonlinear model provides superior predictions to the linear model for  $\Delta u_S$  positive and large. In contrast, for three-dimensional turbulence the prediction of the nonlinear model is no better than the linear model. For two-dimensional turbulence, the probability density functions for the predicted  $\Delta u_S$  from the linear model have an exponential tail, while for the nonlinear model the tail exhibits power law decay. The scaling exponent of this power law can be explained using arguments of the Kolmogorov 1941 theory. Our findings contradict the common assumption that two-dimensional turbulence shares the unpredictability properties of three-dimensional turbulent flows. © 2002 Elsevier Science B.V. All rights reserved.

PACS: 05.45.Tp; 47.27.Gs; 47.27.Jv

Keywords: Turbulence time series; Prediction; Determinism

## 1. Introduction

The discovery of chaos in dynamical systems raised the hope for a better understanding of fluid turbulence. However, turbulence has proved to be too complex to be described by low-dimensional deterministic models with a few degrees of freedom. The common picture instead is of an enormous number of degrees of freedom interacting in a nonlinear fashion, leading to unpredictability on a wide range of time scales. This is an underlying feature of all turbulent flows, includ-

ing homogeneous-isotropic turbulence and large scale atmospheric and oceanic flows, such as the ones modeled by our experiment. In principle, describing the dynamics of a fluid requires solving the Navier–Stokes equations knowing the fluid velocity field  $\vec{u}(\vec{r}, t)$  and the pressure  $p(\vec{r}, t)$  at an initial time  $t_0$ , supplemented by appropriate boundary conditions. One approach to solving the Navier–Stokes equations consists of expanding the fields in a complete set of functions. The amplitudes of these functions then obey an infinite set of ordinary differential equations. Near equilibrium, perhaps only a few modes are excited and all the other modes are irrelevant and enslaved to the excited ones. In this case a few coupled nonlinear ordinary differen-

\* Corresponding author.

E-mail address: ragwitz@mpipks-dresden.mpg.de (M. Ragwitz).

tial equations are sufficient to describe the dynamics of the fluid. Further from equilibrium, however, more and more modes become unstable and the simple description by a few active variables is lost. Indeed, the number of degrees of freedom can be estimated as  $N = (L/\eta)^3$  [1], where  $L$  is the system size and  $\eta$  the Kolmogorov dissipation length.  $N$  can also be related to the Reynolds number  $Re$  through  $L/\eta = Re^{3/4}$  [2]. The number of degrees of freedom is, therefore, expected to be very large at high Reynolds number such as in the atmosphere. Similar arguments should hold for two-dimensional flows with  $N = (L/\eta)^2$ .

The possibility of describing the dynamics of turbulent flows such as the atmosphere by low-dimensional deterministic chaos has led to the *weather/climate attractor conjecture*. Studies supporting this conjecture [3–8] used the Grassberger–Procaccia algorithm [9] and estimated values as low as about five for dynamical dimensions of weather/climate systems. However, in view of the serious data requirements [10], which these studies do not fulfill, these dimension estimates seem unsatisfactory. Recently, Friedrich and Peinke [11] combined the analysis of velocity increments in turbulent systems with a novel approach to stochastic dynamical systems. Their analysis is in terms of spatial scales rather than in the evolution in time and it is not easy to relate their results to ours.

In this paper, we analyze fluid velocity time series measured in a laboratory experiment of turbulent flow in a rapidly rotating annulus, which is designed to model atmospheric dynamics. We obtain linear predictions from an  $m$ th order autoregressive (AR) global model. This model can only capture the linear parts of the dynamics because the predictions do not account for the dependence on the state of the system. In contrast, we find that nonlinear predictions using few-degree-of-freedom low-dimensional models that are *local* in phase space are able to capture part of the dynamics in two-dimensional (2D) turbulence but not in 3D turbulence. Since the dynamic evolution rules fit by a locally linear or locally constant model generally depend on the position in phase space, these schemes can capture globally nonlinear dynamics; this is why we call these algorithms nonlinear models. Although there are no indicators of low-dimensional

attractors in our data, phase space methods developed for deterministic chaotic systems can be used to extract nonlinear structure. The goal of our method is to predict the time series, a time interval  $S$  ahead from the current value  $u(s_n)$  and to calculate the velocity increment  $\Delta u_S = u(s_n + S) - u(s_n)$  between the current point of the time series  $s_n$  and a later time  $S$ .

The goal here is *not* to find an optimal model for turbulence but to obtain data-driven short term predictions. We search for deterministic as well as stochastic contributions. The aim of the paper is to infer the deterministic part, not to develop a model that reproduces the data. The main question of this paper is: do turbulent velocity time series exhibit deterministic structure which goes beyond linear correlations in the data?

The main result of this paper is that for 2D turbulence but not for 3D turbulence, the positive velocity fluctuations ( $\Delta u(s) > 0$ ) predicted by the nonlinear model are closer to the measured values than those predicted by the linear model. Thus nonlinear deterministic structure is present for 2D turbulence but not in the 3D case. Further, in the 2D case the probability distribution function (pdf) of the nonlinearly predicted increments suggests a power law behavior that can be explained using simple scaling arguments.

The rest of the paper is organized as follows. Section 2 describes the experimental apparatus and the measurement techniques. Section 3 presents the algorithms used to predict the experimental data. Section 4 gives a simple numerical example in order to show how the output of the predictors is evaluated. Section 5 discusses the results regarding pdfs, scaling and predictability, and Section 6 is a discussion.

## 2. Experimental methods

Our apparatus is described in [12]. It consists of a rotating annular tank filled with water; the tank is covered with a flat rigid lid and the bottom is conical (to approximate the beta effect, the variation of Coriolis force with latitude). Water is pumped in a closed circuit through two concentric rings of holes in the bottom of the tank (Fig. 1), and this radial flux

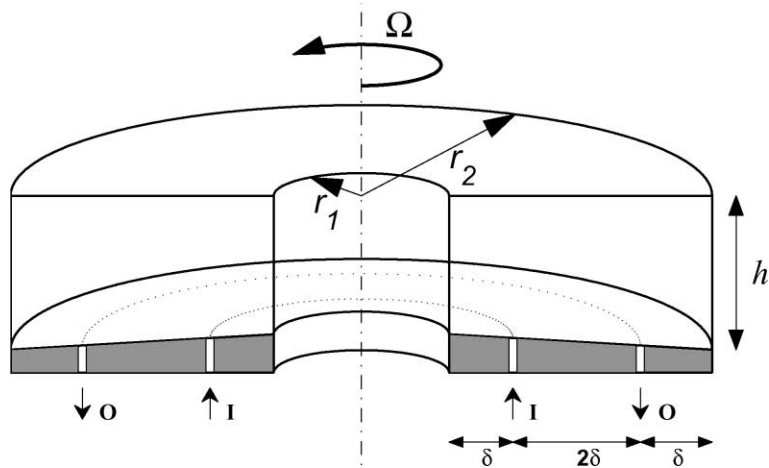


Fig. 1. Cross-section of rotating annulus.  $r_1 = 10.8$  cm,  $r_2 = 43.2$  cm,  $\delta = 8.1$  cm,  $h = 17.1$  cm at  $r_1$ , and  $h = 20.3$  cm at  $r_2$ . I is the inflow, and O is the outflow.

couples with the Coriolis force to generate an azimuthal jet. Here we study the highly turbulent counter-rotating jet generated by strong pumping of the water radially outward. The measurements were made for two sets of control parameters: a quasi-2D flow obtained with  $\Omega = 11.0$  rad/s and  $Q = 150$  cm<sup>3</sup>/s, and at a rotation rate  $\Omega = 1.57$  rad/s and pumping rate  $Q = 450$  cm<sup>3</sup>/s, which yields a more 3D flow (see below).

The pumping flux  $Q$  was made large (450 cm<sup>3</sup>/s) to obtain turbulent flow at the lower of the two rotation rates that we studied. The Reynolds number for this flow was 26,000 based on the peak azimuthal mean velocity  $U$  and a length scale  $L$  equal to the distance between the forcing rings (16.2 cm). The pumping rate at the high rotation rate was made smaller (150 cm<sup>3</sup>/s) so that the Reynolds number (35,000) for the resultant 2D flow would be comparable to that for the 3D flow. The Taylor scale Reynolds number ( $R_\lambda = v_{\text{rms}}\lambda/\nu$ , where  $\lambda$  is the Taylor microscale and  $\nu$  the kinematic viscosity) allows us to better compare with other experiments. Following the definitions given in Ref. [2], we calculate  $R_\lambda^{2D} \simeq 360$ , with  $\lambda_{2D} \simeq 2.0$  cm in the high rotation case. For the low rotation case,  $R_\lambda^{3D} \simeq 360$ , with  $\lambda_{3D} \simeq 1.8$  cm, thus the two states are closely matched.

We measured the flow velocity with hot film probes sampled at a rate of 150 Hz [13]. For each set of control

parameters we obtained six data sets of  $10^6$  points each. The velocity probes were mounted on the top lid and extended a distance of 1 cm into the fluid. The probes were located midway between the inner and outer channel walls, oriented to measure the azimuthal velocity (Fig. 2).

The inertial range dynamics of the flow occur at scales larger than the Kolmogorov dissipation length, defined as  $\eta = (\nu^3/\varepsilon)^{1/4}$ , where  $\varepsilon$  is the energy transfer rate. This rate is estimated by assuming isotropy at small scales; hence  $\varepsilon = 15\nu\langle(\partial u/\partial x)^2\rangle$ . Using these formulas, we estimate the Kolmogorov length  $\eta \simeq 0.07$  cm [13]. The sampling rate  $f = 150$  Hz corresponds to a spatial scale of  $U/f \simeq 0.1$  cm, close to our estimate for  $\eta$ . However, our spatial resolution is limited to 0.3 cm by the length of the probe's sensing element. The velocity data were interpreted using Taylor's hypothesis of frozen turbulence, i.e., temporal fluctuations recorded by the fixed velocity probe should reflect the streamwise spatial fluctuations. The predictions for the velocity increments  $\Delta u_S$  are given in terms of distances  $S = \langle u \rangle t$ , where  $\langle u \rangle$  is the mean velocity.

The importance of rotation is indicated by the Rossby number, defined as  $Ro = U/2\Omega L$ . A small Rossby number indicates a rotation dominated flow, while large  $Ro$  means that inertia is dominant. The Taylor–Proudman theorem shows that, neglecting

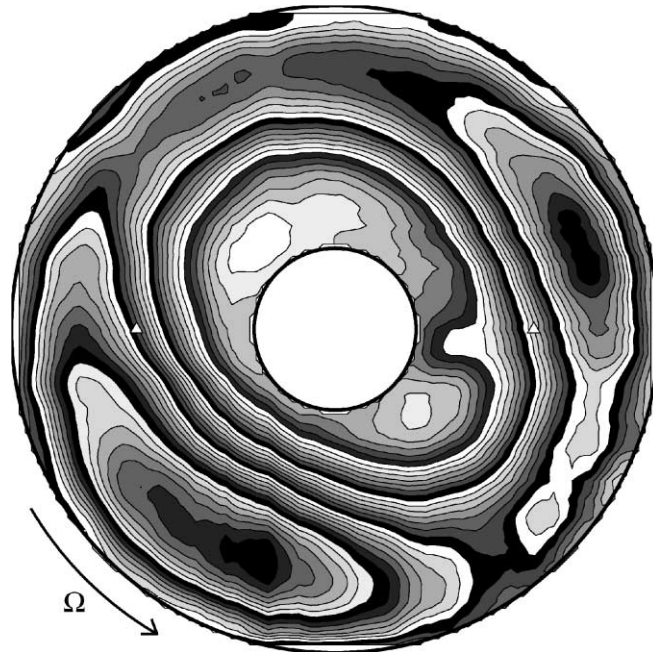


Fig. 2. Streamfunction contours for a 2D flow ( $\Omega = 11.0$  rad/s,  $Q = 150$  cm<sup>3</sup>/s). The locations of the hot film probes are indicated by  $\Delta$ . A rotation rate of  $0.37$  rad/s was subtracted from the  $11.0$  rad/s tank rotation rate to place the observer in the frame rotating at the mean velocity of the flow. In the reference frame of the tank, the cyclonic (dark center) and anti-cyclonic (light center) vortices are advected clockwise by the mean clockwise jet, as the tank rotates counter-clockwise. The closely spaced streamlines in the center of the channel indicate the high velocity jet; the widely spaced streamlines in the vortices correspond to slower velocities.

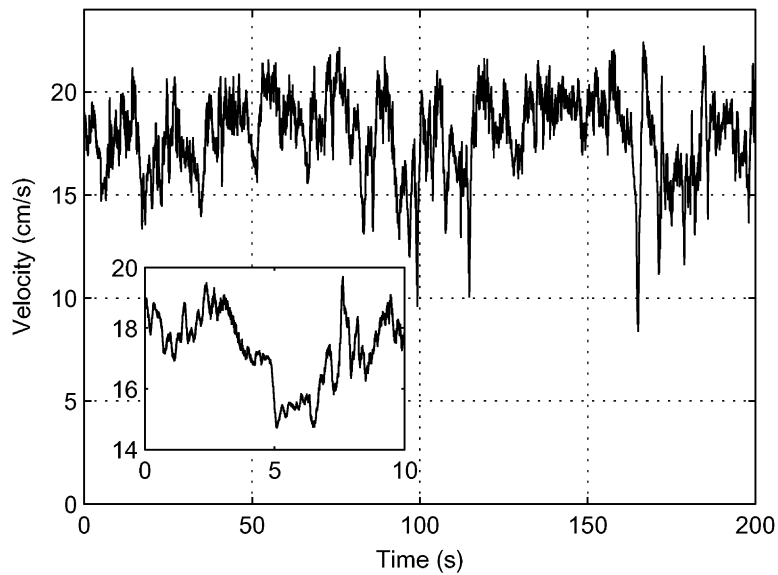


Fig. 3. Typical velocity time series measured at  $\Omega = 11.0$  rad/s and  $Q = 150$  cm<sup>3</sup>/s. The 10 s data segment shown in the inset illustrates the fine turbulent structure superposed on the large fluctuations.

dissipation, in the limit of  $Ro \rightarrow 0$ , the velocity derivatives must vanish in the direction of  $\vec{\omega}$ . For finite but small  $Ro$ , the flow is two-dimensionalized to  $O(Ro)$  [14]. For our data at a high rotation rate (11.0 rad/s), the Rossby number was 0.06, sufficiently low so that the flow was essentially 2D. The flow at the high rotation rate displays self-similar scaling of the structure functions, as expected for a 2D turbulent flow [13]; we refer to this as a 2D flow. In contrast, the Rossby number at 1.57 rad/s was 0.33, large enough so the flow had considerable three-dimensional character. The statistics of this flow are found to show corrections of the structure functions due to scale-dependence, as found for 3D turbulent flows [13]; we refer to this as a 3D flow. Neither flow is isotropic at large scales.

In contrast to co-rotating jets which are strong and narrow, the counter-rotating jet is highly unstable and becomes turbulent even at low pumping flux  $Q$  [15]. The two-dimensionalization, however, is conducive to the formation of long-lived coherent vortices, which are advected clockwise by the mean flow. The velocity at which the vortices travel varies as they interact with the jet and with other vortices; same sign vortices merge while those of opposite sign repel. Compact intense vortices also form in the recirculation regions of the large structures, strongly affecting the motion of the mean flow. As the meandering jet sweeps past the probes, there is a switching between regions of high azimuthal velocity and regions where the flow is primarily in the radial direction. This switching is measured as a dip in the azimuthal velocity, as shown in the time series in Fig. 3.

### 3. Prediction schemes

#### 3.1. Nonlinear model

A classical approach towards nonlinear modeling of aperiodic and apparently unpredictable data is that the scalar time series  $s_n$  obtained by physical measurements is a projection of some phase space vectors  $\vec{x}(t)$  onto the real numbers,  $s_n = h(\vec{x}(t = n/f))$ , where  $f$

is the sampling rate. The assumption of nonlinear time series analysis is that the evolution in this state space is determined by a deterministic, chaotic dynamical system. A variety of tools have been developed for this case [16]. Recently, it has been shown that models originally proposed for deterministic chaotic systems also apply if the underlying dynamics is governed by a Markov process [17]. Let us outline first how phase space models are constructed for deterministic chaotic systems, and then we will show why these algorithms work for Markovian processes as well.

The concept of embedding [18] affirms that in the time delay embedding space of vectors  $\vec{s}_n = (s_n, s_{n-d}, \dots, s_{n-(m+1)d})$  (for  $m$  sufficiently large and appropriate  $d$ ), equations of motion of the form  $s_{n+1} = g(\vec{s}_n)$  exist. The function  $g$  can be reconstructed from the observed data under the assumption of its smoothness. In this paper, we follow Farmer and Sidorowich [19], who introduced locally constant and locally linear approximations of  $g$ . First, a neighborhood diameter  $\epsilon$  has to be fixed and neighborhoods  $\mathcal{U}_n$  of  $\vec{s}_n$  given by  $\mathcal{U}_n = \{\vec{s}_k : \|\vec{s}_k - \vec{s}_n\| \leq \epsilon\}$  are formed. The locally constant predictor (zero-th order) for the unobserved  $s_{n+S}$  is then

$$\hat{s}_{n+S}^{\text{zero}} = \frac{1}{|\mathcal{U}_n|} \sum_{\vec{s}_k \in \mathcal{U}_n} s_{k+S}, \quad (1)$$

the mean of the “futures” of the phase space neighbors. This is the maximum likelihood estimator of  $\hat{s}_{n+S}^{\text{zero}}$  under the assumption of Gaussian errors and a function  $g(\vec{s})$ , which is constant on  $\mathcal{U}_n$ ; hence the name “locally constant predictor”. This can be generalized to a locally linear predictor by replacing  $g(\vec{s}) = \text{constant}$  by  $g(\vec{s}) = \vec{a}\vec{s} + b$ , an affine function.

The central idea of local models is that embedding vectors  $\vec{s}_n = (s_n, s_{n-d}, \dots, s_{n-(m+1)d})$  that are close to each other in phase space follow similar trajectories. The same argument applies if the data are generated by a Markov process of order  $m$ , where only the last  $m$  measurements determine the transition probability for the actual time instance. A scalar Markov process of  $m$ th order in discrete time is defined by the fact that

for any sequence of successive times  $t_1, t_2, \dots, t_n$  with  $n > m$ , all transition probabilities fulfill

$$\begin{aligned}
 & p(s_{n+1}, t_{n+1} | s_n, t_n; s_{n-1}, t_{n-1}, \dots, s_1, t_1) \\
 &= p(s_{n+1}, t_{n+1} | s_n, t_n; s_{n-1}, t_{n-1}, \dots, \\
 & \quad s_{n-m+1}, t_{n-m+1}), \tag{2}
 \end{aligned}$$

i.e., the transition probability depends on the last  $m$  events only. Constructing neighborhoods in delay embedding spaces corresponds to searching for states with similar transition probabilities in the state space of a Markov process. This is the reason why models originally derived for low-dimensional chaotic systems serve as a powerful concept for stochastic Markovian processes as well.

### 3.2. Linear model

The superiority of the locally constant or the locally linear fit over a globally linear fit (an autoregressive model of  $m$ th order AR( $m$ )) of the form

$$\hat{s}_{n+S}^{\text{AR}} = \sum_{i=1}^m a_i s_{n+(1-i)d} \tag{3}$$

is usually interpreted as an indication of nonlinear determinism in the data, formalized, e.g., by the Casdagli test [20].

## 4. Numerical example

In this section, we will discuss the action of the models introduced above when performing predictions on data generated by a nonlinear stochastic process. Before introducing this process we show in Fig. 4 schematically how the data-based predictions are obtained and how our analysis is performed. Both models compute the future value of the time series on the basis of the time series segment of length  $(m - 1)d$ . Using the predicted value  $u(s_n + S)$  the increment  $\Delta u_S = u(s_n + S) - u(s_n)$  between the actual value of the time series and  $u(s_n + S)$  is calculated.

As a numerical example we consider a simple nonlinear stochastic process, a one-dimensional system

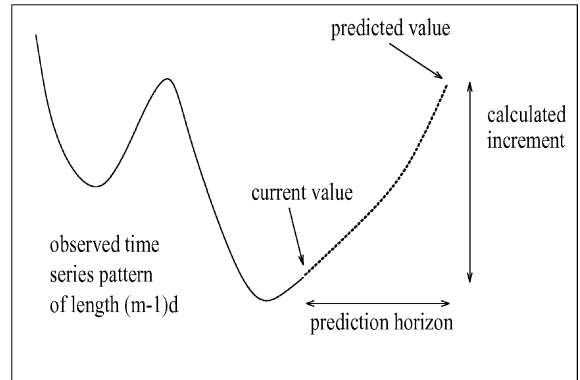


Fig. 4. Schematic picture of the data driven prediction algorithms.

described by the following Langevin equation:

$$\frac{dx}{dt} = \alpha x(t) - x(t)^3 + \beta \Gamma(t) \tag{4}$$

with  $\alpha = 0.1$  and  $\beta = 0.05$ , and  $\Gamma(t)$  is a Gaussian distributed, uncorrelated noise function with vanishing mean. A time series of length  $N = 1,000,000$  was generated by integrating these equations and sampling every 0.1 units of time. An example of a time series of this process is shown in Fig. 5, and the pdfs of the linearly and of the nonlinearly predicted increments  $\Delta \hat{x}_T = \hat{x}_{n+T}^{\text{model}} - x_n$  are shown in Fig. 6. We used the model parameters  $m = 1$  (because the system is one-dimensional) and  $S = 10$ . We also show the pdf of the increments of the actual time series and the

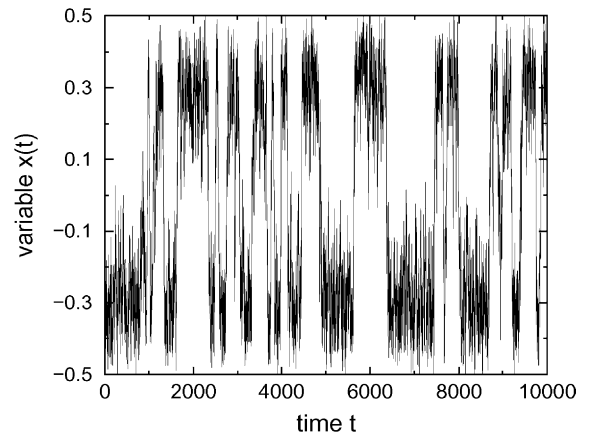


Fig. 5. Time series solution for  $x(t)$  for the Langevin process in Eq. (4) with initial condition  $x(0) = -0.2$ .

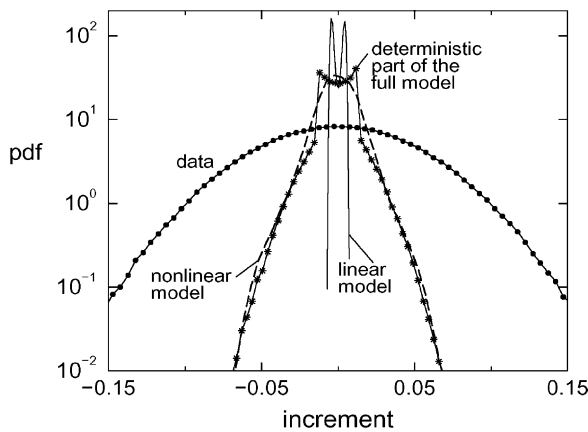


Fig. 6. Pdf of the increments of  $x(t)$  in the system given by Eq. (4). Also shown are the increments predicted by the linear (solid) and by the nonlinear (dashed) model, as well as the increments (\*) predicted knowing the exact deterministic part of the equations of motion.

pdf of the increments if the predictions are performed using the exact deterministic part of the equations of motion (4).

Since the data driven predictors do not know the stochastic inputs  $\Gamma(t)$ , they can in the best case reproduce the deterministic part of the equations of motion. Similarly, one would expect from a good predictor that the statistics of the predicted fluctuations agrees with the statistics knowing the deterministic evolution laws. This is nearly the case here for the pdf of the increments predicted by the nonlinear model, while the AR model is unable to capture the statistics of the deterministic part of the data because the dynamics of this process is nonlinear. Neither predictor is able to reproduce the full pdf of the data since the long tails of that pdf are a combination of nonlinear correlations and the stochastic force  $\Gamma(t)$ , which is unknown by definition. However, the difference between the pdfs obtained from the linear and the nonlinear models indicates nonlinear determinism in the time series. If the main goal of the paper was to reproduce the pdf of the increments of the data one would have to set up a stochastic model using, e.g., the method suggested by Siegert et al. [21]. However, including a stochastic force does not improve predictions on the data, which is the issue of our paper.

## 5. Results

We use the models outlined above to predict velocity increments  $\Delta u_S$  between the future value of the time series and the current value. The application of these models for chaotic deterministic systems requires the choice of optimal embedding parameters. Rigorously, the embedding dimension  $m$  should be  $2\mathcal{D} + 1$ , where  $\mathcal{D}$  is the dynamical dimension of the system [18]. For a Markov process, the embedding dimension should be the order of the process. For our turbulence data we consider the last  $m$  measurements to contain the dominant information on the transition probabilities and the earlier events to be corrections thereof. Our results are presented first with  $m = 10$ , which is large enough to obtain meaningful predictions and small enough to keep the computational effort manageable.

In Section 5.2, we show that varying  $m$  does not affect the qualitative outcome of the results. For a chaotic deterministic system the delay should be of the order of the first minimum of the time delayed mutual information [22]. For a dynamical system of Langevin type the delay should be smaller than this, depending on the noise level [17]. We use the delay that minimizes the mean prediction error. We also show that our results do not depend on a particular choice of the delay  $d$ ; we use values corresponding to distances between 2 and 8 mm. The prediction horizon  $S$  is chosen to be between 20 and 80 mm in order to match its size with the length of the embedding vectors.

### 5.1. Pdf's of the predicted velocity increments

The probability density functions (pdf's) of the measured velocity increment, the linearly predicted increment, and the nonlinearly predicted increment for 2D turbulent flow are shown in Fig. 7. There is a clear asymmetry for the nonlinearly predicted increments: the negative increments predicted by the nonlinear model decay almost as fast as those predicted by the linear model, but the positive ones decay much more slowly. Since the large positive increments will lead us to deterministic structure in 2D turbulence, we consider only the positive branch of the pdf's in the

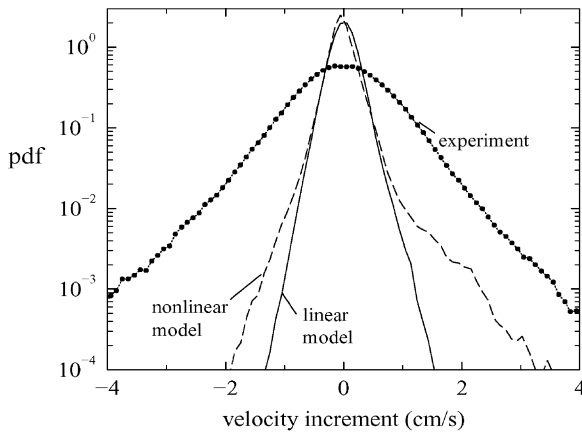


Fig. 7. Pdf's of the measured velocity increment  $\Delta u_S$ , the linearly predicted increment, and the nonlinearly predicted increment for 2D turbulent flow with  $m = 10$ ,  $d = 2$  mm, and  $S = 20$  mm.

remainder of this work. A discussion of the observed asymmetry will be given at the end of Section 5.

The pdf's for 3D and 2D flows are shown in Fig. 8 for positive velocity increments for the same model parameters as in Fig. 7. The pdf's of the increment of the measured time series depend on the distance  $S$ , as discussed in [13]. For 3D turbulence the pdf has exponential tails for small values of  $S$  and becomes approximately Gaussian for large  $S$ . For 2D flows the dependence of the pdf on  $S$  is weaker; for a wide range of distances  $S$  it exhibits exponential decay. A log–log plot (not shown) suggests power law behavior of the tails of the pdf for large increments in the 2D flow. For the intermediate value of  $S = 20$  mm used in Fig. 8, both pdf's decay approximately exponentially.

The behavior of the predicted velocity increment is different in 2D and 3D flow. In the 3D case the pdf's obtained from the nonlinear model as well as from the linear model decay exponentially (see Fig. 8). Consequently, the time series only contains linear correlations; all other fluctuations are anticipated as noise by both models. In the 2D, flow the predictions of the two models differ. The pdf of the increments predicted by the linear model still decays exponentially. However, in the nonlinear case the decay is slower, suggesting a power law behavior for large increments, as will be discussed in Section 5.3.

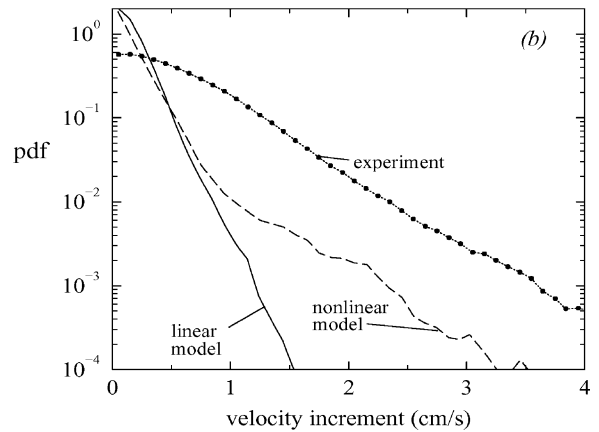
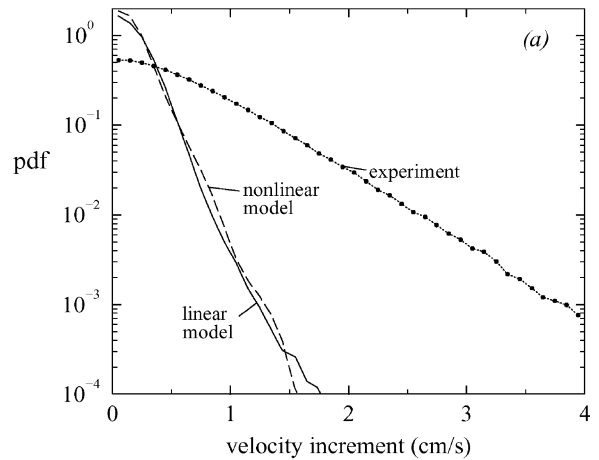


Fig. 8. Pdf's of the positive velocity increment from the experiment, the linear model, and the nonlinear model for: (a) 3D flow, and (b) 2D flow with  $m = 10$ ,  $d = 2$  mm, and  $S = 20$  mm.

The discrepancy between the experimental pdf and the pdf predicted by the nonlinear model is due to the stochastic part of the dynamics, which cannot be captured by any predictor, as discussed for a simple example in Section 4. To put it differently, this difference has its origin in the fact that modeling and predicting are very distinct tasks in stochastic dynamical systems. Our aim here is prediction. The difference between the nonlinear model and the linear one suggests the existence of nonlinear correlations in the data, which will be discussed in Section 5.4. This difference will lead us to nonlinear determinism in the data, because it corresponds to a better performance

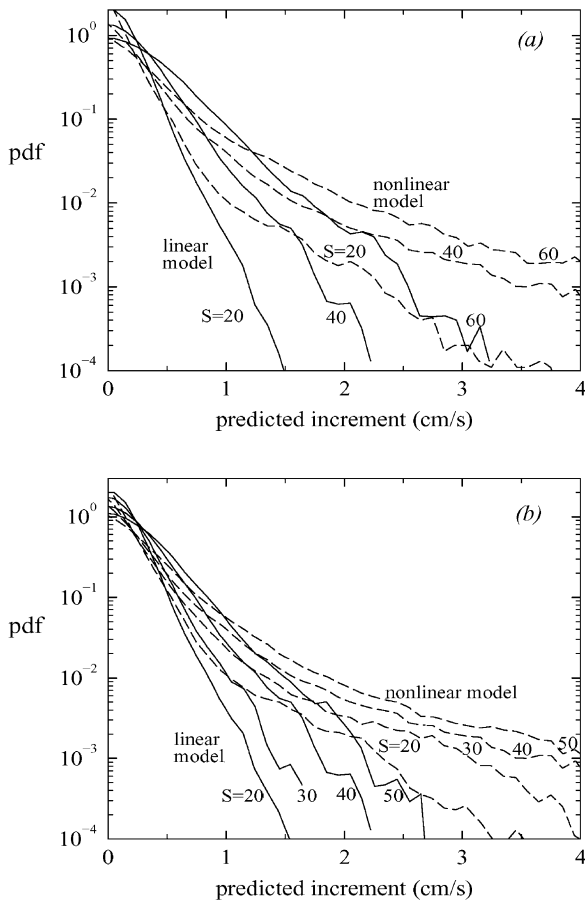


Fig. 9. Pdf's of the velocity increment for 2D turbulence from the linear model (solid line), and the nonlinear model (dashed line) for (a)  $m = 5, 10, 15$  with  $d = 4$  mm and  $S = 20, 40, 60$  mm, and (b)  $d = 2, 3, 4, 5$  mm with  $m = 10$  and  $S = 20, 30, 40, 50$  mm.

of the nonlinear model in situations when a strong increase of the velocity occurs.

### 5.2. Dependence on parameters

We now show that the qualitative structure of the pdf for 2D turbulence does not depend on the model parameters  $m$  and  $d$ . First we vary the embedding dimension  $m = 5, 10, 15$ , and keep  $d$  fixed by also varying the respective prediction horizons,  $S = 20, 40, 60$  mm, as shown in Fig. 9(a). Next we examine different delays,  $d = 2, 3, 4, 5$  mm, keeping  $m$  constant at  $m = 10$  (so  $S = 20, 30, 40, 50$  mm), as

shown in Fig. 9(b). For all parameter values the increments predicted for 2D turbulence by the nonlinear model decay more slowly and qualitatively differently from those predicted by the linear model.

### 5.3. Scaling

We have shown in Section 4 that, for a stochastic system, one cannot expect the pdf's of the predicted increments and of the increments of the experimental data to be in close agreement. The same is true for the turbulence data since in turbulent velocity time series one always expects a stochastic contribution due to unresolved degrees of freedom. Because the noise inputs are unknown they cannot be captured by any predictor of the type discussed here. The difference between linearly and nonlinearly predicted increments is a sign for nonlinear correlations in the data. Is it possible to understand the functional form of the pdf of the increments predicted by the nonlinear model?

We have noted that the pdf for the 2D flow for large velocity increments is suggestive of power law decay (see Fig. 8(b)). This can be understood when analyzing the action of the nonlinear predictor. Let us first discuss *when* the large positive increments, that correspond to the power law behavior, are predicted. In Fig. 10, the average pattern of the velocity signal is shown for a situation when the nonlinear model predicts an

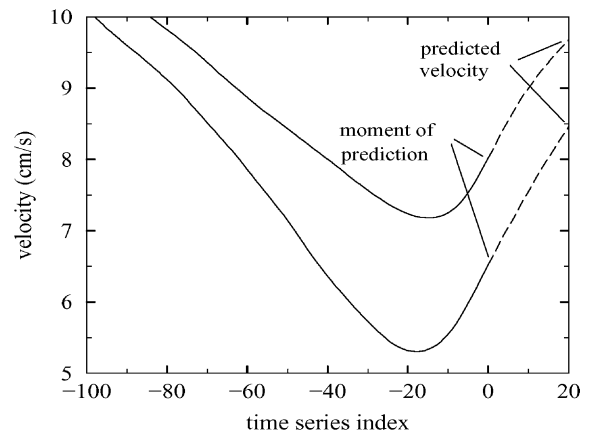


Fig. 10. Average velocity pattern when positive increments of 1.5 cm/s (upper curve) and 2 cm/s (lower curve) are predicted by the nonlinear model with  $m = 10$ ,  $d = 2$  mm and  $S = 20$  mm.

increase in the velocity of 1.5 or 2 cm/s. It can be seen that before a large increment is predicted the signal passes through a pronounced minimum. As we know from Section 2 these minima correspond to coherent vortices. Thus a large positive increment is predicted when a large coherent vortex passes the probe.

Now let us discuss *how* the increase is predicted. The nonlinear predictor makes its prediction by searching for all patterns in the time series that possess a similar structure, and then averaging over the “futures” of these patterns. The patterns of the form shown in Fig. 10 are supposed to represent coherent vortices of a certain size  $r$ . Therefore, the nonlinear predictor computes the *average* velocity increase after a vortex of a particular size  $r$  has passed the detector. To every vortex of size  $r_0$  the average velocity increment  $\langle \Delta u_r \rangle_{r=r_0}$  for vortices of this size is attached. The number of vortices of size  $r_0$  is, therefore, directly translated into the number average velocity increments of size  $\langle \Delta u_r \rangle_{r=r_0}$ .

We will see now in the second step that the distribution of the vortices is indeed a power law, which agrees with the observed behavior. A prediction of power law behavior can be obtained by assuming scale invariance and using results of the Kolmogorov 1941 (K41) theory [2]. Scale invariance predicts the distribution of vortices of size  $r$  in a turbulent fluid to scale as  $r^{-3}$  in 3D flow and as  $r^{-2}$  in 2D flow, to assure that eddies of different size fill the same volume. Since our measurements are performed in only one spatial dimension, we take the cross-sections of different vortices into consideration. Then along a one-dimensional line the number of eddies should scale as  $r^{-1}$  in 2D as well as in 3D turbulence. The relation between the size of the vortex and its average velocity increment is given by the K41 theory. The theory predicts that the longitudinal velocity structure functions  $\langle (\Delta u_r)^n \rangle = \langle (u(x+r) - u(x))^n \rangle$  are given by

$$\langle (\Delta u_r)^n \rangle = C_n \varepsilon^{n/3} r^{n/3},$$

where  $\varepsilon$  is the energy dissipation rate per unit mass and  $C_n$  a universal constant. The physical content of the Kolmogorov theory is that the typical velocity increment within eddies of size  $r$  behaves as  $\varepsilon^{1/3} r^{1/3}$  [23]. This gives us the desired relation for the pdf of

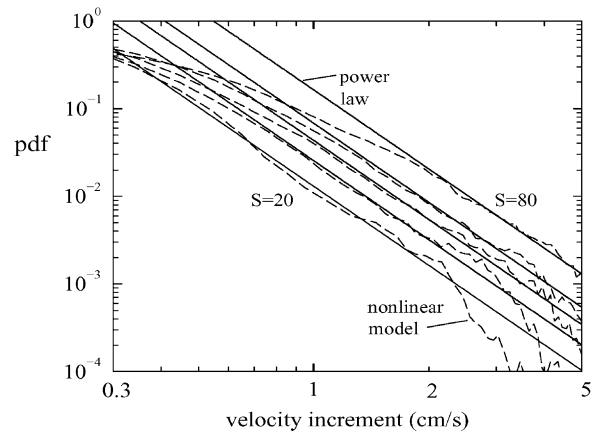


Fig. 11. Comparison of the pdf of the nonlinearly predicted velocity increments (dashed lines) with the power law scaling deduced from the Kolmogorov theory (solid lines). The different curves correspond to different embedding parameters, from bottom to top:  $d = 2, 3, 4, 5, 8$  mm and  $S = 20, 30, 40, 50, 80$  mm.

the number of vortices versus their typical velocity increment  $\Delta u_r$ : it should scale as  $\Delta u_r^{-3}$ .

The pdf for nonlinearly predicted velocity increments is compared with the Kolmogorov power law  $\Delta u_S^{-3}$  for large velocity increments and different prediction horizons in Fig. 11. The pdf's exhibit the predicted scaling for a range of nearly one decade. The onset of the scaling region is shifted towards larger velocity increments for longer prediction horizons and longer embedding vectors. This is expected since vortices that are smaller than the sum of the prediction horizon and the length of the embedding vector can no longer be resolved by the predictor. For the largest displayed values, this sum reaches a length of about 16 cm, which corresponds roughly to the largest coherent structures in our system and consequently a pronounced scaling region is no longer observed.

#### 5.4. Degree of determinism

In the preceding sections we have seen for the 2D flow that the nonlinear model predicts more large fluctuations of the velocity signal than the linear model and that the statistics of the nonlinearly predicted increments are closer to that of the actual data. However, this statistics does not tell us whether the large

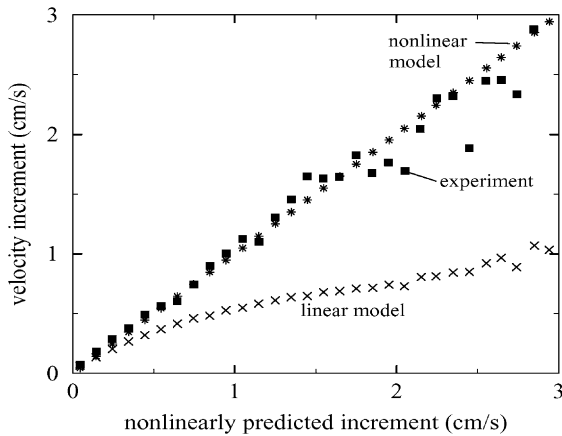


Fig. 12. The nonlinearly predicted increment (stars) agrees well with the measured velocity increment (solid squares), while the linear model (crosses) systematically underestimates the increments (2D flow with  $S = 20$  mm).

increments are predicted in situations when large fluctuations actually occur in the data. Are the large increments, predicted by the nonlinear model, correlated in time with the increments of the data, and do they lead to increased predictability of the nonlinear scheme? Which model gives the better predictions in the region of the pdf where the two models differ? These are the questions we want to answer in this section. In Fig. 12, we show the average of the observed increment  $\Delta u_S$  in situations when an increment  $\Delta \hat{u}_S$  is predicted by the nonlinear model for the 2D flow. We also show the increments predicted by the linear model for these situations. While the measured increments coincide on average with the predictions of the nonlinear model, the linear model systematically underestimates the fluctuations. This again is a sign of the presence of nonlinear structure in the data (see Fig. 10)).

In 3D flow we observe the opposite behavior for nonlinear versus linear prediction, i.e., the nonlinear model performs worse on average for large predicted velocity increments. This is shown in Fig. 13, where the relative improvement of the nonlinear scheme over the linear model,  $I = (E_{\text{zero}} - E_{\text{AR}})/\Delta u$ , is displayed for 2D and 3D flow. Here  $E_{\text{zero}}$  and  $E_{\text{AR}}$  are the averaged absolute prediction errors of the nonlinear (zeroth order) and the linear model (AR model), respectively. While the improvement is positive for large predicted

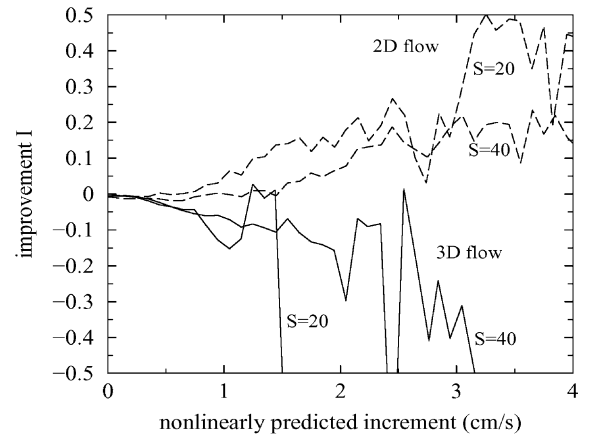


Fig. 13. The relative improvement  $I$  of the nonlinear model versus the linear scheme for 2D (dashed line) and 3D (solid line) flow as a function of the size of the nonlinearly predicted increment ( $m = 10$ ;  $d = 2, 4$  mm;  $S = 20, 40$  mm).

velocity increments in 2D, it is negative for 3D turbulence. This shows not only that we do not find nonlinear structure in 3D velocity time series, but also that the linear model is even superior due to the limited statistical robustness of the locally constant scheme.

Finally, we emphasize the asymmetry between positive and negative velocity increments (Fig. 7). Neither the scaling behavior nor the exponential decay of the relative prediction error can be detected for negative velocity increments. This behavior can be understood in the following way: the large negative increments are due to the radial flow as a vortex sweeps the probe, which then produces a large positive increment. The negative increment cannot be predicted because one does not know whether the vortex will pass through the probe or if it will miss it. Once it has passed through, however, we can predict the upcoming positive velocity increment.

## 6. Discussion

We have analyzed the dynamics of two-dimensional and three-dimensional turbulent flow by linear and nonlinear modeling of velocity time series. For 2D turbulence we found that nonlinear phase space models can have predictive power superior to linear models

when the velocity increments are positive and large. A similar improvement of the nonlinear model has been observed earlier for atmospheric surface wind data [24]. We also found that the pdf of the nonlinearly predicted increments in the 2D case scales like  $\Delta u^{-3}$ , as expected from the Kolmogorov theory if one assumes a scale invariant distribution of vortices. For 3D turbulence we found that the nonlinear model was no better than the linear model. An intuitive reason for the difference between 2D and 3D flow is the absence of a vortex stretching term in a 2D fluid. This stretching allows the dynamics within a 3D vortex to be much more complicated than those of a 2D vortex.

## Acknowledgements

The work at the University of Texas was supported by a grant from the US Office of Naval Research and the work at the Max-Planck Institut für Physik komplexer Systeme in Dresden was supported by a grant from the German Federal Ministry of Economics.

## References

- [1] L.D. Landau, E.M. Lifshitz, Fluid Mechanics, Pergamon Press, Oxford, 1959.
- [2] U. Frisch, Turbulence, Cambridge University Press, Cambridge, 1995.
- [3] K. Freidrich, J. Atmos. Sci. 43 (1986) 419.
- [4] C.L. Keepenne, C. Nicolis, J. Atmos. Sci. 46 (1989) 2356.
- [5] C. Nicolis, G. Nicolis, Nature 326 (1987) 523.
- [6] G. Poveda-Jaramillo, C.E. Puente, Boundary-Layer Meteorol. 64 (1993) 175.
- [7] A.A. Tsonis, J.B. Elsner, Nature 333 (1988) 545.
- [8] M.B. Sharifi, K.P. Georgakakos, I. Rodriguez-Iturbe, J. Atmos. Sci. 47 (1990) 888.
- [9] P. Grassberger, I. Procaccia, Phys. Rev. Lett. 50 (1983) 346.
- [10] A. Wolf, J.B. Swift, H.L. Swinney, J.A. Vastano, Physica D Sec. 7 16 (1985) 285; J.P. Eckmann, D. Ruelle, Physica D 56 (1992) 185.
- [11] R. Friedrich, J. Peinke, Phys. Rev. Lett. 78 (1997) 863.
- [12] T.H. Solomon, W.J. Holloway, H.L. Swinney, Phys. Fluids 5 (1993) 1971.
- [13] C.N. Baroud, B.B. Plapp, Z.S. She, H.L. Swinney, Anomalous self-similarity in two-dimensional turbulence, submitted for publication, ar Xiv:physics/0104055.
- [14] D. Tritton, Physical Fluid Dynamics, Oxford Science Publications, Oxford, 1993.
- [15] J. Sommeria, S.D. Meyers, H.L. Swinney, Nature 337 (1971) 58; J. Sommeria, S.D. Meyers, H.L. Swinney, Experiments on Vortices and Rossby Waves in Eastward and Westward Jets, in: A. Osborne (Ed.), Nonlinear Topics in Ocean Physics, 1988, pp. 227–269.
- [16] H.I. Abarbanel, Analysis of Observed Chaotic Data, Springer, New York, 1996; H. Kantz, T. Schreiber, Nonlinear Time Series Analysis, Cambridge University Press, Cambridge, 1997.
- [17] M. Ragwitz, H. Kantz, Markov models from data by simple nonlinear time series predictors in delay embedding spaces, to appear in Phys. Rev. E (2002).
- [18] F. Takens, Lecture Notes in Mathematics, Vol. 898, Springer, New York, 1981; T. Sauer, J. Yorke, M. Casdagli, J. Statist. Phys. 65 (1991) 579.
- [19] J.D. Farmer, J.J. Sidorowich, Phys. Rev. Lett. 59 (1987) 845; J.P. Crutchfield, B.S. McNamara, Complex Syst. 1 (1987) 417; E.J. Kostelich, J.A. Yorke, Phys. Rev. A 38 (1988) 1649.
- [20] M. Casdagli, Physica D 35 (1989) 335.
- [21] S. Siebert, R. Friedrich, J. Peinke, Phys. Lett. A 243 (1998) 275.
- [22] A.M. Fraser, H.L. Swinney, Phys. Rev. A 33 (1986) 1134.
- [23] K. Gawedzki, Easy Turbulence. *chao-dyn/9907024 v2*.
- [24] M. Ragwitz, H. Kantz, Europhys. Lett. 51 (2000) 595.